Impact of water plasticization on dialcohol cellulose fibres melt processing-structure-properties relationship

Carbohydrate Polymer Technologies and Applications 9 (2025) 100642

Contents lists available at ScienceDirect

Carbohydrate Polymer Technologies and Applications

journal homepage: www.sciencedirect.com/journal/carbohydrate-polymer-technologies-and-applications

Impact of water plasticization on dialcohol cellulose fibres melt processing-structure-properties relationship

Enrica Pellegrino [a,b], Basel Al-Rudainy [c], Per A. Larsson [d], Alberto Fina [b], Giada Lo Re [a,*]

[a] Chalmers University of Technology, Department of Industrial and Materials Science, SE-412 96 Gothenburg, Sweden
[b] Politecnico di Torino, Department of Applied Science and Technology, 15121 Alessandria, Italy
[c] Lund University, Department of Chemical Engineering, SE-221 00 Lund, Sweden
[d] KTH Royal Institute of Technology, Department of Fibre and Polymer Technology, SE-100 44 Stockholm, Sweden

ARTICLE INFO

Keywords:
Thermoplastic cellulose fibres
Melt processing design
Polyolefin replacement
Cellulose derivative
Processing-structure-properties relationships

ABSTRACT

Cellulose and its derivatives are considered sustainable alternatives to non-biodegradable fossil-based plastics. Chemically modified cellulose fibres to dialcohol cellulose (DAC) fibres demonstrated a melt processing window between the glass transition and degradation temperatures which enabled their extrusion by using only water as a temporary plasticizer. With the aim of supporting an industrial upscale of DAC fibres, this study investigates the processing design and the feasibility of melt processing, minimizing the moisture. Melt processes-structure-properties relationships were studied by varying the sequence of primary and secondary melt processes, *i.e.,* extrusion and injection moulding, and by changing the moisture content. The effect of moisture and processing design on the fibre structural properties, such as molecular weight, crystallinity, fibre morphology and fibre suspensions rheology, was assessed. Then, the thermomechanical behaviour of the 3D-shaped DAC injected materials was correlated with DAC fibres structural features obtained by the different processing design and moisture content. Our results identified the injection moulding as a milder process for achieving the preparation of 3D-shaped material with enhanced mechanical properties. Moreover, we disclosed the relevance of controlled moisture in the extrusion process for enabling a secondary shaping directly after compounding and the possibility of 3D-shaping DAC fibres after a rehydration step.

1. Introduction

The increasing world population and the standard of living are leading to growing demand and utilization of plastic materials for different applications. In 2021, worldwide plastic volumetric production was estimated to be around 391 million metric tons (Statista, 2021). Fossil-based and non-biodegradable plastics lead to significant environmental problems, as waste management and recycling methods are inadequate (Li et al., 2022). The replacement of this plastic with biodegradable products from renewable resources seems to be a good alternative, in particular, for the substitution of disposable plastic. In 2021, the main utilization of bioplastic accounts for the replacement of fossil-based plastic in disposable food packaging applications (European Bioplastics, 2021).

Owing to growing environmental awareness, cellulose, the world's most abundant biopolymer, has received increasing attention from the scientific community to replace fossil-based and non-biodegradable plastic. Besides being biodegradable and renewable, cellulose provides a complex hierarchical structure that develops from the nanoscale to the macroscale, providing high mechanical properties at relatively low density (Li et al., 2022). The establishment of a hierarchical structure is closely linked to the strong intermolecular forces present between the cellulose chains (Li et al., 2023; Wohlert et al., 2023). However, these interactions limit the possibility of producing such material using the melt processing methods commonly used for plastics, as it starts to significantly degrade before reaching the molten state (Li et al., 2022). These methods allow the production of 3D-shaped packaging materials, which are useful for fabricating certain food packaging products, such as caps and bottles, which cannot be obtained by paper manufacturing methods. Also, the high number of hydroxyl groups within cellulose chains results in the material's strong sensitivity to water and moisture, an aspect that limits the use of cellulosic materials in some food

* Corresponding author at: Rannvagen 2A SE-412 96 Gothenburg, Sweden.
E-mail addresses: enricap@chalmers.se (E. Pellegrino), rudainy@chemeng.lth.se (B. Al-Rudainy), perl5@kth.se (P.A. Larsson), alberto.fina@polito.it (A. Fina), giadal@chalmers.se (G. Lo Re).

https://doi.org/10.1016/j.carpta.2024.100642

Available online 15 December 2024

packaging applications (Liu et al., 2021).

Melt processing of cellulose, a solvent-free production method, could be obtained by developing strategies that allow the disruption of the intermolecular interactions due to hydrogen bonds (Li et al., 2022). Under some ideal conditions, using a combination of mechanical shear, pressure, and with or without laser radiation, cellulose can be softened (Schroeter & Felix, 2005; Zhang, Wu, Gao & Xia, 2012). However, these methods are energy-demanding and lead to materials with lower mechanical properties, compared to the native cellulose, due to the destruction of the hierarchical structure and crystalline domains.

To facilitate the melt processing of cellulose, small mobile molecules that can intercalate between cellulose chains decreasing mutual interactions, *i.e.* plasticizers, can be used. However, the amount of plasticizer required to be effective for melt processing results in a composite in which the matrix is the plasticizer. This strategy does not fully exploit the cellulose potential. For example, ionic-liquid-plasticized cellulose materials were prepared with microcrystalline cellulose adding 1-butyl-3-methylimidazolium chloride as a plasticizer for the compression moulding of cellulose, leading to a material with inferior mechanical properties (Wu, Bai, Xue, Liao, Zhou & Xie, 2015).

To improve the mobility of the cellulose chains, controlled chemical modification of cellulose has also been explored to convert hydroxyl groups to esters and ethers. However, the melt processing of these cellulose derivatives is highly dependent on the degree of substitution and remains challenging because of a narrow gap between glass transition (T_g) and degradation temperatures, *i.e.* narrow processing window (Li et al., 2022). Therefore, large amounts of plasticizers are still needed to facilitate melt processing. Moreover, this technique may lead to a greatly reduced crystallinity, which, together with the need for the use of plasticizers, reduces the mechanical properties of the final product.

Grafting polymers or copolymers onto cellulose has been also used to enhance cellulose thermoplastic processability (Li et al., 2022). However, this strategy required a high grafting ratio, resulting in fragile materials with decreased thermal stability.

One promising solution for the melt processing of cellulose is the chemical modification of cellulose fibres into dialcohol cellulose (DAC) fibres. Selective oxidation to dialdehyde cellulose followed by reduction to form DAC (Zeronian, Hudson & Peters, 1964) allowed the melt processing of cellulose fibres only by using water as a temporary plasticizer (Engel, Lo Re & Larsson, 2024; Lo Re et al., 2023; Mehandzhiyski, Engel, Larsson, Lo Re & Zozoulenko, 2022). The oxidation reaction is performed with sodium periodate, which can selectively cleave the C_2–C_3 bonds in the glucopyranose backbone of cellulose, and the following reduction with sodium borohydride converts the so formed aldehydes into hydroxyl groups (Zeronian, Hudson & Peters, 1964). After the oxidation step that leads to the formation of dialdehyde cellulose the glucopyranose ring opens, forming at the fibres surface two aldehyde moieties per ring opening. These moieties are highly reactive and unstable already at room temperature making them a green crosslinker (Münster et al., 2017). The opening of the glucose units of cellulose, followed by the reduction, leads to a more flexible structure compared to the one of native cellulose. Considering the degree of modification (DOM) as the percentage of open C_2–C_3 bonds, assuming that the starting material is pure cellulose, the higher the DOM the lower the T_g of the DAC assessed by differential scanning calorimetry (DSC) and dynamic-mechanical analysis (DMA), implying a widening of the processing window (Kasai, Morooka & Ek, 2014). Moreover, a decrease in crystallinity due to the partial conversion of cellulose to DAC was observed and assigned to the conversion of crystalline to amorphous domains (Larsson, Berglund & Wågberg, 2014). It is proposed that the oxidation reaction using periodate proceeds gradually from the surface to the core of each nanofibril and aggregate thereof (Guigo, Mazeau, Putaux & Heux, 2014). Therefore, it has been hypothesized that this modification could lead to the creation of a core-shell structure, composed of a core of crystalline cellulose and a shell of amorphous DAC (Larsson, Berglund & Wågberg, 2014). This conversion allows the material to maintain part of the mechanical properties provided by the highly ordered cellulose while simultaneously increasing the flexibility of the fibres and their bonding to each other (Larsson, Berglund & Wågberg, 2014).

The presence of many hydroxyl groups in the structure of cellulose leads to strong interactions between water and cellulose (Larsson, Berglund & Wågberg, 2014). After the modification to DAC, the number of hydroxyl groups remains the same, while the mobility of the system increases, due to the lower crystallinity of the system: the increased amorphicity leads to an increased number of exposed hydroxyl groups, so it is observed in greater moisture sorption (Larsson, Gimåker & Wågberg, 2008). Water has been demonstrated to play the role of a temporary plasticizer (Engel, Lo Re & Larsson, 2024; Lo Re et al., 2023; Mehandzhiyski, Engel, Larsson, Lo Re & Zozoulenko, 2022) having an even more pronounced effect by increasing the DAC DOM, an effect that can be observed by DMA analyses performed at different relative humidity, *i.e.* at different content of moisture in the samples (Larsson, Berglund & Wågberg, 2014; Salmén & Larsson, 2018). With the increase of relative humidity, a significant reduction in storage modulus is observed, connected to the material T_g. The T_g is observed at lower relative humidities for higher DOMs.

Water acts as a green plasticizer, temporarily lowering the T_g favouring the DAC melt processing (Larsson, Berglund & Wågberg, 2014). However, water partially evaporates during melt processing and/or storage (Lo Re et al., 2023). If only the water at the equilibrium (23 °C and 50 % relative humidity (RH)) is kept (~ 6 wt.%) the 3D-shaped materials are expected to perform high mechanical properties. With the aim of easing an industrial uptake of melt processed DAC fibres, the investigation of the minimum moisture content enabling primary and secondary 3D-shaping is of interest. This would allow for the minimization of the energy consumption needed to evaporate water and obtain dense solid materials.

Under the hypothesis that different levels of plasticization (*i.e.* initial moisture content) would change DAC fibre structural features upon melt processing, this study investigates the DAC fibre processing-structure-properties relationships enabling a suitable production of 3D-DAC parts with maximised performance. Moreover, we postulate an influence of the exposure to thermomechanical stresses during the melt processing on the structural changes and final properties of the 3D parts. Therefore, the study includes the design of the melt processing steps towards the production of dense 3D-DAC parts by performing a primary process, *i.e.* melt compounding, followed by a secondary process, *i.e.* injection moulding, consecutively or inserting a rehydration step. The two designs simulate the production of 3D-shaped materials directly after the pelletization or when the secondary shaping is performed later in a different industry. The two steps are compared with a single-step process of injection moulding. Targeting fossil-based plastic replacement for disposable packaging, we aim for the production of dense (~ 6 wt.% moisture content at the equilibrium), complex 3D-shaped structures from DACfibres, which cannot be obtained by conventional papermaking techniques. The study provides a deeper understanding of the mechanism of interaction between water and DAC, which can enable its effective manufacturing in 3D products with controlled properties. Moreover, this work demonstrates how production methods typical of fossil-based plastics, *i.e.* extrusion and injection moulding, can be reliable for DAC fibres, and will serve for the design of other ways to plasticize DAC that could overcome water drawback, *e.g.* DAC water sensitivity.

2. Materials and methods

2.1. Dialcohol cellulose (DAC) and its properties

DAC with a 46 % DOM, derived from bleached softwood kraft pulp fibres, was supplied by BillerudKorsnäs (Solna, Sweden) in the form of sheets (at equilibrium moisture content of 6 wt.%). In Table S1 are

reported the physical-chemical characterization of pristine bleached softwood kraft pulp fibres, including purity and sugar analysis. The chemical modification was obtained following the method previously reported by Larsson et al. (Larsson & Wågberg, 2016; Larsson, Berglund & Wågberg, 2014). Sodium periodate was used to partially oxidize cellulose into dialdehyde cellulose, breaking the C_2-C_3 bond in the glucopyranose ring. The oxidation was followed by a reaction using sodium borohydride that allows for the reduction of the aldehyde groups in alcohol groups (Fig. S1). The degree of modification (DOM) was evaluated by the aldehyde content after periodate oxidation following a well-established protocol based on reaction with hydroxylamine hydrochloride (Zhao & Heindel, 1991). Considering all the aldehyde groups to be reduced, a 46 % DOM was estimated. The apparent weight (M_w~80,000 Da) and number (M_n~30,000 Da) average molecular weights and dispersity values (Đ~2.7) were estimated using a size exclusion chromatography (SEC) in N,N-dimethylacetamide containing 8 % LiCl (LiCl/DMAc). The same method was used to evaluate the molecular weight of DAC after the different melt processing designs. For the materials production, deionized water was added to the sheets (with a known equilibrium moisture content of 6 wt.%) to achieve the desired moisture content before the melt processing.

2.2. Determination of the moisture content

The moisture content of samples, evaluated after each processing step, was assessed by drying samples for 48 h in an oven at 70 °C. The temperature has been set to 70 °C to be milder to the fibres and enable rehydration in some of the further experiments. Measurements were performed in triplicates and reported as mean values.

2.3. Melt compounding and injection moulding of materials with different moisture contents

Different fabrication paths were used to prepare the samples for this study (Fig. 1). First, for all the materials, the water addition needed to obtain the desired initial moisture content before the melt compounding, or the injection moulding, was calculated. The amount of additional water was evaluated considering the required amount of dry solid DAC (20 g for melt processing and 12 g for injection moulding) to process and the moisture content possessed by DAC before the process. The material feed during compounding was prepared by cutting sheets into thin strips (width ≈ 50 mm) and weighting them. The strips were placed in sealed glass bottles and the required amount of water was added (using a pipette) drop by drop evenly over the strips. The glass bottles then were sealed for a minimum of 24 h to absorb the water fully and evenly.

After desired hydration, the strips were primarily melt compounded in a micro-compounder (Fig. 1a) and injection moulded following two paths: by direct injection moulding (Path 1, Fig. 1b) and by indirect injection moulding (Path 2, Fig. 1c). For the path of indirect injection moulding, there was a second hydration step to increase the moisture content that the materials had after compounding to a fixed amount. As an alternative process path, one set of strips was only processed by direct injection moulding (*i.e.* no melt compounding) (Path 3, Fig. 1d). The melt compounding was performed in an Xplore micro-compounder (Xplore, Maastricht, The Netherlands). The following processing conditions were used: temperature 100 °C, residence time 15 + 5 min (feeding + compounding), screws speed 15 + 60 rpm (feeding + compounding), and dry solid DAC 20 g. Table 1 provides sample names and

Table 1
Moisture content changes before and after melt compounding and injection moulding. The number before DAC refers to the initial moisture content before the compounding. The number after DAC refers to the moisture content before injection moulding. In the direct path (_dir) the compounding is directly followed by injection moulding, and in the indirect path (_ind) a rehydration has been inserted between the two processes. Injection moulded materials without a previous compounding are referred as injDAC.

Material	Initial moisture content [wt.%] *Melt compounding*	Final moisture content [wt.%]	Moisture loss during [g]
40 DAC	40 ± 2	30 ± 2	4.8 ± 1,9
35 DAC	35 ± 2	25 ± 2	4.1 ± 1,7
30 DAC	30 ± 2	20 ± 2	3.6 ± 1,5
25 DAC	25 ± 2	15 ± 2	3.1 ± 1,3

	Initial moisture content [wt.%] *Injection moulding*	Final moisture content [wt.%]
40 DAC 30_dir	30 ± 2	28 ± 2
40′ DAC 30_ind	25 ± 2	24 ± 2
25 DAC 30_dir	30 ± 2	27 ± 2
injDAC 40	40 ± 2	36 ± 2
injDAC 30	30 ± 2	29 ± 2
injDAC 25	25 ± 2	23 ± 2

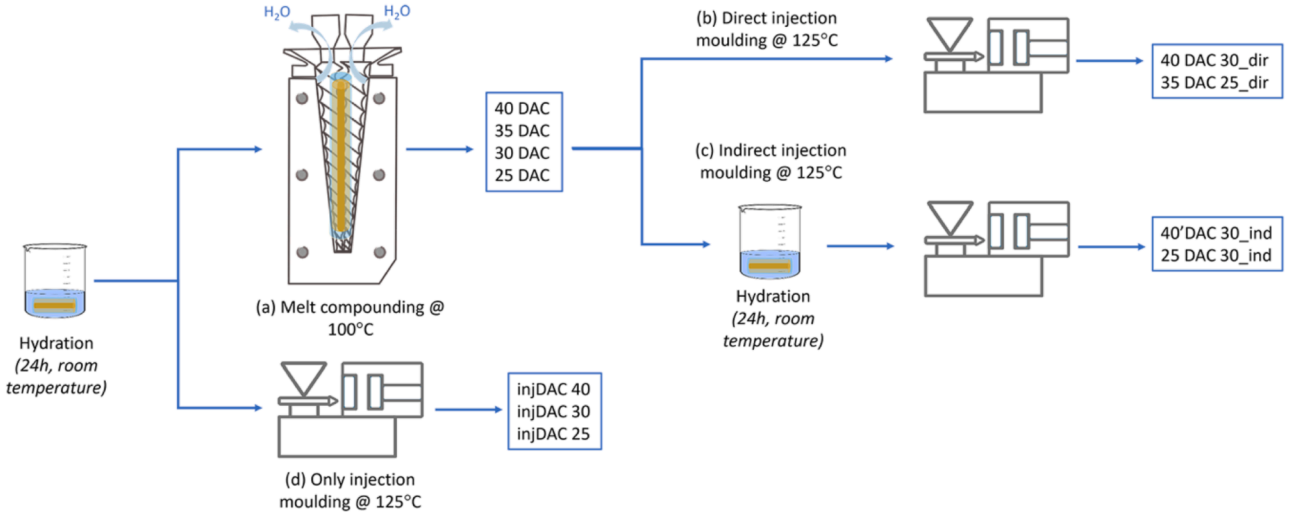

Fig. 1. Scheme of the equipment and methodology (paths) used for the melt processing of DAC. The number before DAC refers to the initial moisture content before the compounding. The number after DAC refers to the moisture content before injection moulding. In the direct path (_dir) the compounding is directly followed by injection moulding, and in the indirect path (_ind) a rehydration has been inserted between the two processes. Injection moulded materials without a previous compounding are referred as injDAC.

their variation in moisture content before and after the process. In the name of the samples, the number is related to the different initial moisture content used for the melt compounding (weight percentage, wt.%).

The injection moulding was performed in an Xplore micro-injection moulding equipment (Xplore, Maastricht, The Netherlands). Even in this case, several processing conditions were used: temperature of the injector 125 °C, temperature of the mould 30 °C, pressure imposed on the material was 7 bar for 25 s, and dry solid DAC 12 g. Table 1 provides sample names and their variation in moisture content before and after the process.

A mould suitable for producing rectangular bars ($10 \times 60 \times 1$ mm^3) has been selected according to standard ISO 294. In the name of the samples, the first number is (still) the initial moisture content used for the melt compounding and the second number is the moisture content used for the injection moulding. Direct and indirect injection moulding are indicated by _dir, and _ind, respectively, injDAC refers to materials injection moulded without any prior compounding.

2.4. Torque and melt viscosity

During the compounding, the micro-compounder registered the torque imposed on the co-rotating screws, and from these values, the equipment software calculated the melt viscosity according to Eq. (1).

$$\eta = \frac{\tau}{\dot{\dot{\gamma}}} \tag{1}$$

where $\ddot{\gamma}$ is the shear rate (recorded by the equipment) and τ is the shear stress (proportional to the torque).

2.5. Apparent molecular mass by size exclusion chromatography

The apparent molecular mass (if dissolved partial DAC behaves like the conventional pullulan standards used for native cellulose) was determined by size exclusion chromatography (SEC). To facilitate such measurement, the DAC fibres were first dissolved in N,N-dimethylacetamide (DMAc) containing 8 % LiCl (LiCl/DMAc). This was achieved by first soaking 80 mg of the sample in 10 ml of water to swell the fibres. Then, four equivolumetric solvent exchanges to ethanol were performed, followed by four equivolumetric solvent exchanges to dewatered DMAc, and finally, removal of excess DMAc to have DMAc-saturated fibres. An 8 % LiCl/DMAc solution was prepared by heating DMAc at 120 °C for 60 min. Once the DMAc had cooled to about 70 °C, oven-dried LiCl was added. The solution was left overnight to ensure complete dissolution of the LiCl. Once all LiCl was dissolved, the DMAc-saturated fibres were added to 10 ml of 8 % LiCl/DMAc and left under overnight magnetic stirring to dissolve the DAC fibres. Finally, once the fibres were visually dissolved, the solutions were diluted for SEC analysis with LiCl-DMAC to solutions containing 1.6 % LiCl and a cellulose content of 1.2 g/l.

The molecular weight distributions of the DAC samples were ultimately determined by More Research (Örnsköldsvik, Sweden) in an Aligent PL-GPC 220 (CA, Santa Clara, USA) SEC system equipped with three 20 μm mixed-A columns from Polymer Labs, one guard column and two 300 mm columns connected in series, and a refractive index detector. The system was calibrated with eight Polymer Lab pullulan standards with molecular weights ranging from 6.1 kDa to 708 kDa. The mobile phase used was 0.5 % LiCl/DMAc at a temperature of 70 °C and a flow rate of 1.0 ml/min.

2.6. X-Ray diffraction

X-Ray diffraction (XRD) spectra were recorded by a D8 Discover Diffractometer (Bruker AXS, Karlsruhe, Germany) with Cu Kα radiation (40 kV, 40 mA) in a 2θ range between 10° and 40° Crystallinity was quantified through the relative crystallinity index (CrI), calculated according to Eq. (2).

$$CrI = \frac{I_{002} - I_{am}}{I_{002}} \tag{2}$$

CrI was calculated according to the method developed by Segal et al. (Segal, Creely, Martin Jr & Conrad, 1959), calculating the ratio between the crystal peak indexed as (200) (I_{002}) at $2\theta = 22.5°$ subtracted by the "amorphous" contribution given by the minimum intensity between the peaks indexed as (200) and (110) (I_{am}) (at $2\theta = 18.5°$ (Park, Baker, Himmel, Parilla & Johnson, 2010; Segal, Creely, Martin Jr & Conrad, 1959), divided by I_{002}.

Before XRD measurements all samples were stored for 48 h at equilibrium conditions (23 °C and 50 % RH).

2.7. Fibres size and size distribution

Fibre length distribution analyses were performed using a Kajaani FS300 fibre analyser (Metso Automation, Kajaani, Finland). This device is specifically designed to evaluate the fibre length distributions of cellulosic fibres (Carvalho, Ferreira, Martins & Figueiredo, 1997). Measurements are based on the ability of these fibres to change the direction of polarized light (Mörseburg, Hultholm, Lundin & Lönnberg, 1999). It is worth noting that, in the case of DAC this measurement is considered indicative of the relative size changes, because of the limitations in precisely capturing the water swollen part of the modified fibres. The samples were prepared by suspending 10 mg of material in 100 ml of deionized water by gentle agitation. The values of length weighted average length (L_l), length weighted average width (W_l) and percentage of fines ($Fines_l$) were obtained from the equipment.

2.8. Scanning electron microscopy

Fibre morphology analysis was performed, before and after processing, using an Ultra 55 FEG Scanning Electron Microscope (SEM) (Zeiss Sigma, Oberkochen, Germany). To prepare the samples, 0.01 % fibre suspensions were poured into glass containers and freeze dried, using an Alpha 1–2 LDplus freeze dryer (GmbH, Osterode, Germany). This technique allowed us to observe isolated cellulose fibres and fragments, as well as some aggregates resulting from sample preparation. The isolated fibres were then attached to a conductive carbon tape and then sputtered with a thin layer of gold, at 1.5 kV and 18 mA for one minute, using an edwards sputter coater s150b (Edwards Vacuum, Burgess Hill, England).

2.9. Rheological analyses

Rheology analysis was performed at room temperature using an MCR 300 rheometer (Anton Paar, Graz, Austria), equipped with a vane (six blades) in a smooth cup system (vane: ST34/2 V/30/156, $d_{vane} = 34$ mm, cup: CC39/T200/XL/SS, $d_{cup} = 42$ mm), also supplied by Anton Paar. The vane system was chosen due to its lower solid depletion at the wall and lower apparent slip effects (Mohtaschemi, Sorvari, Puisto, Nuopponen, Seppälä & Alava, 2014; Nechyporchuk, Belgacem & Pignon, 2016; Schenker, Schoelkopf, Gane & Mangin, 2018,; 2019). The samples were obtained by suspending 5 g of material in 100 ml of deionized water by gentle magnetic stirring for 24 h. After loading the samples and immersing the vanes, the system was left to rest for 2 min before the beginning of the measurements, without applying any pre-shearing. Flow curves were obtained by an automated shear rate increase ramp from 0.01 to 1000 s^{-1}. A total of 30 log-equidistant-distributed point measurements were performed per ramp in an automated acquisition time mode and shear rate control. The viscoelastic behaviour was assessed by an amplitude sweep measurement at a frequency of 0.5 Hz. The automated strain-amplitude-controlled ramp was set from 0.01 to 1000 % with 60

log-equidistant-distributed point measurements and automated acquisition time mode. Rheological analyses were used to study the effect of different fibres morphology on fibres dispersions rheological behaviour.

2.10. Water release evaluation

A sample mass of about 300 mg of dry substance was introduced into a 50 ml centrifugal tube along with 20 ml of deionized water. The mixture underwent agitation using a vortex mixer (MS2 Minishaker, IKA-Werke GmbH & Co. KG, Staufen, Germany) at 2500 rpm for at least 5 min or until any material clumps were no longer visible. Subsequently, the solid and liquid phases were separated using a centrifuge (Sigma 3–16 K, Sigma Laborzentrifugen GmbH, Osterode am Harz, Germany) operating at 4000 rpm and room temperature for 30 min. After removing the liquid phase through decantation, the solid material was placed in a cylindrical mould and shaped into a disk with a diameter of 26.5 mm. The subsequent step involved the drying process, employing a moisture analyser (MBT 163 M, VWR International LLC, Radnor, Pennsylvania, USA) set to 45 °C. The drying criterion was defined as a weight change of <0.05 % over a minimum period of 90 s. The obtained data, depicting moisture content over time, underwent polynomial fitting and was then transformed into free moisture content and drying rate curves according to Eqs. (3) and 4.

$$Free\ moisture\ content = \frac{m_{start} - m_{end}}{m_{end}} \tag{3}$$

$$Drying\ rate = -\frac{m_{end}}{A} * \frac{d(Free\ moisture\ content)}{dt} \tag{4}$$

where m_{start}, m_{end}, A, t denotes the initial mass, final dry mass, drying area (551 mm^2) and time, respectively.

2.11. Dynamic mechanical thermal analysis

Dynamic mechanical thermal analysis (DMTA) was performed with a Q800 DMA (TA Instruments, Delaware, U.S.) operating in the tensile mode, to study the viscoelastic nature of the analysed materials produced. The oscillation frequency and amplitude were 1 Hz and 10 μm, respectively, and temperature scans were performed at a rate of 3 °C/min in the temperature range of 30–190 °C. The materials, before being tested, were for 48 h at equilibrium conditions (23 °C and 50 % RH). The test was performed on injected materials obtained using the three different production methods (direct, indirect, and only injection).

3. Results and discussion

3.1. Melt compounding and injection moulding with different initial moisture contents

For a given type of DAC fibres, the glass transition (T_g) influences the melt processability, *i.e.* the processing window between the T_g and degradation temperature. Two parameters determine the T_g: the degree of modification (DOM) and the moisture content (Engel, Lo Re & Larsson, 2024; Lo Re et al. 2023; Mehandzhiyski, Engel, Larsson, Lo Re & Zozoulenko, 2022). In this study, we kept the DOM constant (46 %), while controlling the initial moisture content in both extrusion and injection moulding.

Different paths were followed to process DAC with different initial moisture contents (summarised in Fig. 1) to assess the lowest amount of water required to have a good and reproducible melt processing.

To elucidate the effect of water during the DAC melt processing, both on compounding and on injection moulding, we performed a gravimetrical analysis to assess the moisture content after the two processing steps. The starting DAC fibres were stored and conditioned at 23 °C and 50 % relative humidity (RH), resulting in a moisture content of 6 wt.%. To these fibres, placed in sealed glass bottles, a controlled amount of water was added to reach a total moisture content of 25, 30, 35 and 40 wt.%. The processing conditions have been selected taking into consideration previous literature (Engel, Lo Re & Larsson, 2024). Table 1 reports the changes in moisture content before and after melt compounding and injection moulding.

Fibres of all different initial moisture contents could successfully be compounded; images of extrudates can be seen in Fig. S2. The measured in-line melt viscosity (Fig. 2a) and torque values (Fig. 2b) were lower than the safety limit of the micro-compounding equipment; the greater the moisture content, the lower the torque and the melt viscosity. The water disrupts the interactions between the DAC fibres, resulting in a decrease in the viscosity during the compounding. An initial moisture content of about 25 wt.% was identified to approach a minimal amount required for a stable compounding process, as the melt viscosity (Fig. 2a) shows high values, and the torque (Fig. 2b) was close to the limit of the equipment (45 Nm).

Conceivably, the overall decrease in melt viscosity during compounding can be ascribed to fibres orientations in the direction of melt flow, while the local small increases to locally reduced mobility of fibres due to their entanglement in the melt (Fig. 2a).

The processing temperature was set at 100 °C, and some water was expected to evaporate. Therefore, the moisture content before and after the melt compounding was measured (Table 1). The moisture content change, *i.e.* loss of water, decreases by decreasing the moisture content before compounding, due to a lower amount of water in contact with the environment. The moisture content after compounding lowers while decreasing the initial moisture content and this would be relevant considering the following injection process.

After compounding, two different paths have been followed, based on the moisture content and the melt properties. The moisture contents for direct and indirect injection moulding are considered as the moisture contents owned by the material without or with the addition of water after compounding (Table 1 and Fig. 1b and c). These two paths were compared together with samples injection moulded without any prior compounding. For 40 DAC 30_dir, compounded with 40 wt.% initial moisture content and directly injected (Fig. 1b), a stable, *i.e.* reproducible, injection process was observed (Fig. 2c). The extruded material still contained 30 wt.% of water before the injection moulding, affording a suitable melt viscosity to completely fill the mould for all the subsequent injections (injection frequency of 1 injection every 2 min). At lower initial moisture content, 35 DAC 25_dir, the extruded material possessed a higher melt viscosity and a less stable direct injection process (Fig. S3). This shows that 25 wt.% of water was not sufficient to allow a desirable injection process. Therefore, for melt compounded fibres with lower initial moisture contents an indirect injection moulding was investigated (Fig. 1c). To decrease the melt viscosity and enable complete filling of the mould, the extrudates were rehydrated to a sufficient moisture content before the injection. Specifically, the material compounded with the lowest initial moisture content (25 wt.%) was rehydrated up to 30 wt.% of moisture content before the injection. However, somewhat unexpectedly, it was not possible to have a stable injection process (Fig. 2e) for 25 DAC 30_ind.

To further investigate the path of rehydration of lost water before injection moulding, compared to the direct injection moulding, a material containing 30 wt.% of moisture content after compounding (*i.e.* compounded with an initial moisture content of 40 wt.%) was dried in an oven (at 70 °C for 48 h) and rehydrated up to a moisture content of 30 wt.% before injection moulding (40′ DAC 30_ind). This resulted in a stable injection process (Fig. 2d). This suggests that is the initial moisture content before compounding that affects the material injectability and not the rehydration step as 25 DAC 30_ind was not stably injectable unlike 40′ DAC 30_ind. Under the hypothesis that is the moisture content during the compounding step that impacts the injectability of the material, the third path (Fig. 1d) was investigated, *i.e.* the strategy in which materials with different initial moisture contents (25–40 wt.% of moisture content) were injected, without any prior compounding. A stable

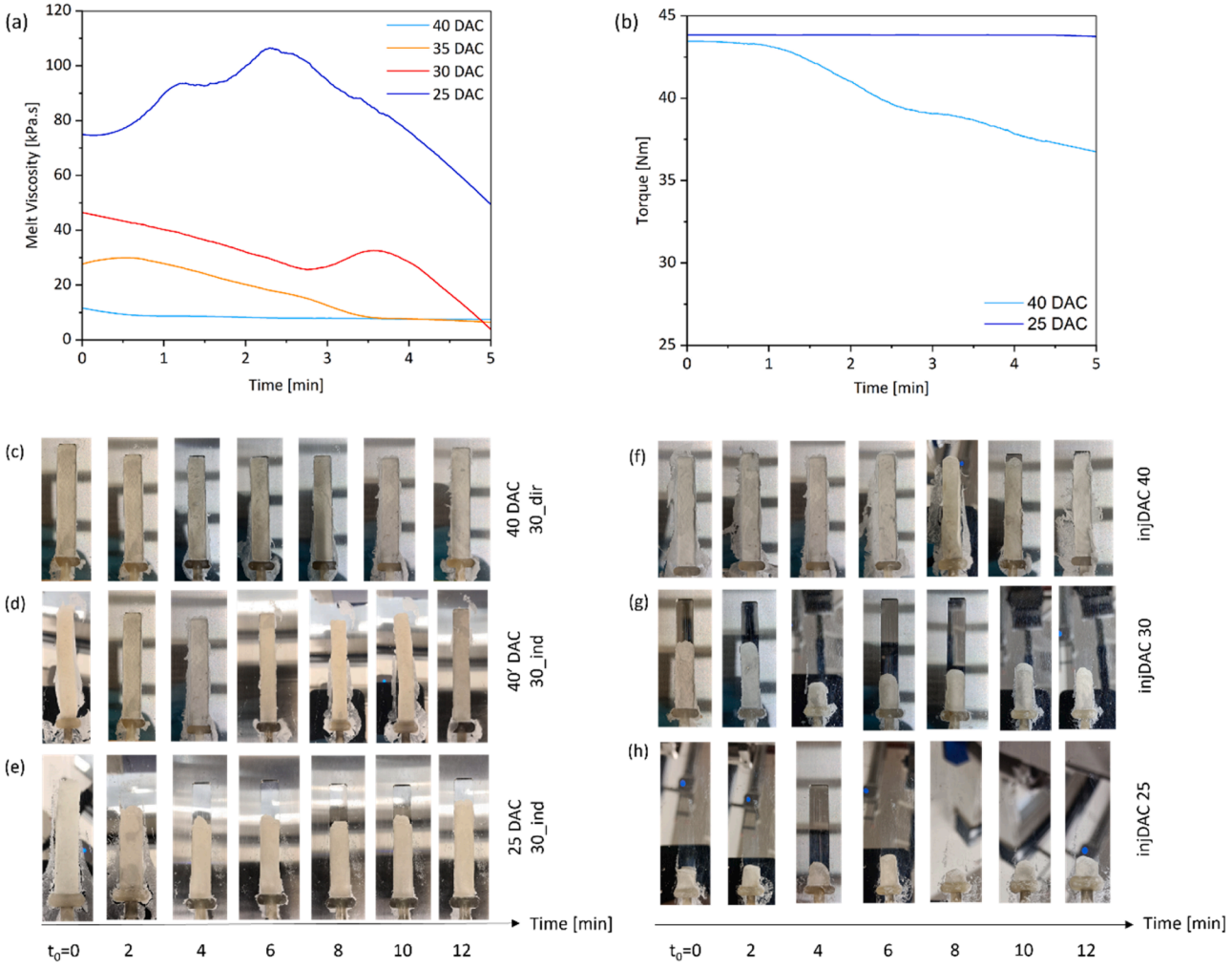

Fig. 2. (a) Melt viscosity and (b) torque registered by the equipment during 5 min of compounding. The photos show subsequent injection of the materials, performed every 2 min (after 5 min of compounding): (c) 40 DAC 30_dir, (d) 40′DAC 30_ind, (e) 25 DAC 30_ind, (f) injDAC 40, (g) injDAC 30, (h) injDAC 25. Sample naming is explained in Fig. 1.

injection process was observed for injDAC 40 (Fig. 2f) but not for injDAC 30 (Fig. 2g) or injDAC 25 (Fig. 2h), which both showed unstable injection processes.

The material melt compounded with the highest moisture content (40 wt.%) exhibits a stable injection starting from a moisture content of 30 wt.%, both directly and indirectly; this behaviour is not observed for the material melt compounded with the lowest moisture content (25 wt. %) and the unprocessed material, which would need more water to have a stable injection process.

Different cellulose structural properties affect cellulose interactions with water (Aulin et. al, 2009). Therefore, we hypothesized that different amount of initial moisture content, leading to different melt viscosity and shear stresses during compounding, affects the supramolecular ordering of DAC fibres, and so its interactions with water and injectability. To study the effect of moisture content during compounding on DAC fibres, the structural properties of the resulting materials were compared with those achieved by only injection moulding.

3.2. *Effect of processing on fibre structure and morphology*

3.2.1. *Apparent molecular weight*

To better understand the processing-structure-properties relationship of DAC fibres, we first investigated whether different initial moisture contents and processing methods would lead to cellulose degradation, by evaluating possible changes in weight (M_w) and number (M_n) average molecular weights and polydispersity values (Đ). Cellulose degrades *via* the breakage of glycosidic, inter-monomer bonds in the polymer (Emsley, Ali & Heywood, 2000). Size exclusion chromatography (SEC) in N,N-dimethylacetamide (DMAc) containing 8 % LiCl (LiCl/DMAc) (a non-degrading solvent for cellulose and DAC) provided information on the M_w, M_n and Đ of cellulose giving detailed information about changes in molecular structure (Emsley, Ali & Heywood, 2000; Westermark & Gustafsson, 1994). Larsson et al. (Larsson, Berglund & Wågberg, 2014) investigated how the chemical modification from bleached softwood kraft fibres to DAC affects the molecular weight distribution. After the modification, DAC chromatograms show a shift of the peaks of the molecular weight frequency distribution towards the left, *i.e.* towards higher molecular weights. In addition, Đ halved (from 11 to ≈ 6) and the molecular weight distribution appears more symmetric. These findings are explained by the yield loss during DAC fibres production, due to the progress of the chemical modification. It is further proposed little chain scission taking place during limited DOM.

In contrast with Larsson et al., more recent studies (Mystek et al., 2020; Simon et al., 2023), evidenced a stronger effect on the molecular weight: the average molecular weight shows an exponential decrease as the DOM of the DAC increased. These results can be explained by an evident β-elimination process that could compete with a reduction reaction, leading to chain degradation (Simon et al., 2023).

The SEC chromatograms obtained after the DAC compounding and injection moulding, starting from different initial moisture contents

(lowest and highest water content before compounding for 40 DAC and 25 DAC and highest water content before the only injection for injDAC 40, Fig. S4) show how the molecular weight distributions remain almost unchanged after the different processing steps. The measured M_w and M_n exhibit a slight change while Đ remain constant (Table S2). These comparative results show that the different processing steps, performed starting from different initial moisture contents, *i.e.* different viscosities leading to different shear stresses during the processing on the DAC fibres, do not noticeably influence the DAC chains scission. The processing could influence the fibres morphology, such as average fibre length, length distribution, fibrillation, and DAC crystallinity. Therefore, further structural analyses were carried out to evaluate these features.

3.2.2. X-ray diffraction

Cellulose has a highly ordered structure, in which the symmetry and hydroxyl moieties lead to the creation of strong intra- and intermolecular London dispersion interactions (Li et.al, 2023) and hydrogen bonds interactions (Park, Baker, Himmel, Parilla & Johnson, 2010), dispersed into disordered amorphous regions.

Modification of native cellulose to DAC has shown a decrease in crystallinity proportional to the increase in the degree of modification (Larsson, Berglund & Wågberg, 2014). The effect of the different production methods (direct, indirect, and only injection) on the crystallinity was evaluated through X-Ray diffraction (XRD) analyses (Fig. 3a).

Cellulose I is characterised by five main peaks at ≈ 14.9°, 16.5°, 21.2°, 22.5° and 34.5°, related to (1–10), (110), (102), (200) and (400) crystallographic planes, respectively (French, 2014). The peaks indexed as (1–10), (110) and (200) are clearly visible in most cellulose samples, whereas the (102) may appear as a shoulder (Martínez-Sanz, Pettolino, Flanagan, Gidley & Gilbert, 2017). The peak at 34.5°, represents a broad peak indexed as (400) although it is a composite of several neighbouring peaks (French, 2014). In our unprocessed DAC scattering peaks at 2θ of 14.9°, 16.5°, 22.5° and 34.5°, typical of cellulose I (French, 2014), are observed; however, the peak at 21.2°, is not visible (Fig. 3a).

To directly compare our results with Larsson et al., we applied the same method (proposed by Segal et al.) for the calculation of the relative crystallinity index (CrI). This method only considers the intensity of the peaks indexed as (200), acceptable for comparing the relative differences between materials. To assess the total crystalline and amorphous contributions in modified cellulose samples (Park, Baker, Himmel, Parilla & Johnson, 2010) the contribution to the calculation of (1–10), (110) and (400) crystalline planes should be considered.

Compounding had a stronger effect on reducing the crystallinity of the compounded DAC fibres, as clearly seen by comparing materials compounded (40 DAC 30_dir, 40′ DAC 30_ind and 25 DAC 30_ind) and not compounded before (injDAC 40, injDAC 25) the injection moulding (Table 2). Compared to unprocessed DAC, even injection moulding leads to a decrease in crystallinity, milder than the compounding effect. Compared to the other peaks, the one indexed as (110) (≈ 16.5°) decreases more in intensity after compounding, but not further after the only injection moulding. The shear forces imposed on the material lead to a partial distortion of the (110) plane crystallinity possibly due to a preferential orientation in the flow direction.

XRD results demonstrate that the reason for the different injectability of injDAC 40 and injDAC 25 cannot be ascribed to a change in the crystallinity.

It is proposed that the mobility of DAC relies mainly on amorphous regions, and the DAC melt processing involves the flow of a (nano) composite with perfect interface, where the matrix is the amorphous region in which (nano)crystalline regions are dispersed. However, the obtained results cannot resolve the inherent challenge of nanofibril/fibre level of modification, and therefore mobility.

3.2.3. Fibre length distribution

The effect of melt processing, including both compounding and injection moulding, on the fibre length and the presence of fines, which are defined as fibres smaller than 0.2 mm (Mörseburg, Hultholm, Lundin & Lönnberg, 1999), was evaluated using a fibre analyser.

To investigate the effect of compounding of DAC fibres on the fibre morphology, the materials obtained with the highest and lowest initial

Table 2
Summary of the results obtained by X-Ray diffraction analysis and dynamic mechanical thermal analysis performed on 40 DAC 30_dir, 40′ DAC 30_ind, 25 DAC 30_ind, injDAC 40 and injDAC 25: crystallinity index (assessed according to Segal et al. (Segal, Creely, Martin Jr & Conrad, 1959), storage modulus at 30 °C ($E'_{@\ 30\ °C}$), 150 °C ($E'_{@\ 150\ °C}$) and the glass transition temperature (T_g).

Material	CrI	$E'_{@\ 30\ °C}$ [GPa]	$E'_{@\ 150\ °C}$ [GPa]	Moisture content [wt.%]	T_g [°C]
DAC	64	/	/	6 ± 1	/
40 DAC 30_dir	47	0.97	0.04	6 ± 1	69
40′ DAC 30_ind	49	0.92	0.04	6 ± 1	70
25 DAC 30_ind	46	0.93	0.05	6 ± 1	69
injDAC 40	59	2.10	0.09	8 ± 1	63
injDAC 25	58	1.42	0.07	6 ± 1	70

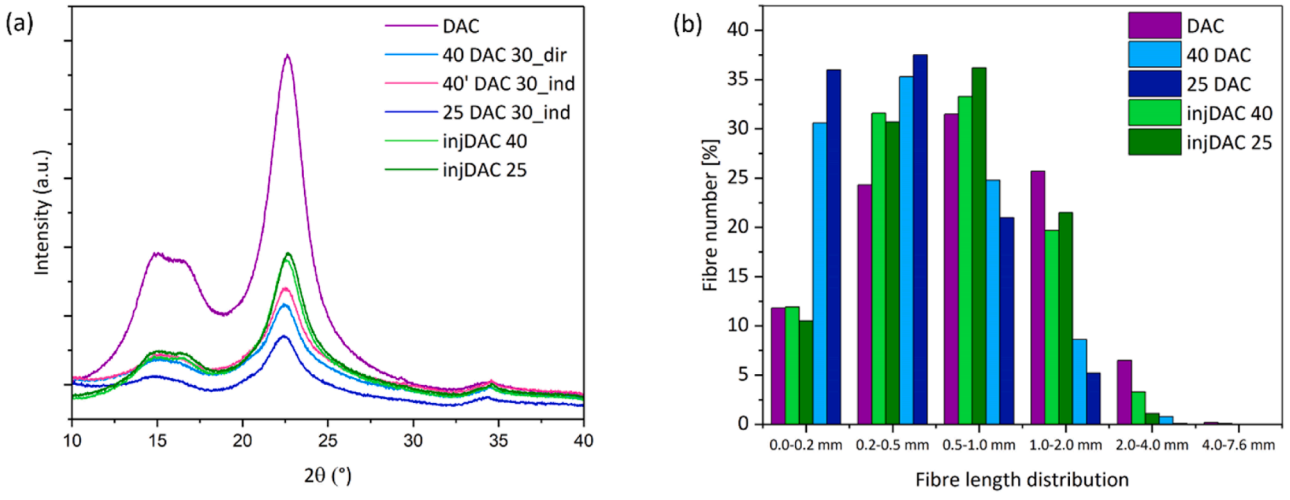

Fig. 3. (a) XRD patterns of unprocessed DAC fibres, 40 DAC 30_dir, 40′ DAC 30_ind, 25 DAC 30_ind, injDAC 40 and injDAC 25. (b) Length-weighted fibres length distribution of unprocessed DAC, 40 DAC, 25 DAC, injDAC 40 and injDAC 25.

moisture contents (40 DAC and 25 DAC) were tested. Compared to the unprocessed DAC, 40 DAC and 25 DAC present a decrease in the average fibre length (L_l) and aspect ratio, and an increase in the percentage of fines (Table 3).

This shortening of the fibres is stronger for 25 DAC, compounded with a lower initial moisture content (Fig. 3b). The initial moisture content hence affects the length distribution of the fibres during compounding. A lower moisture content leads to a higher melt viscosity, connected to a higher torque to flow the fibres, *i.e.* a concomitant higher shear stresses on the fibres. This explains the further reduction (from 44 % for 40 DAC to 56 % for 25 DAC) in average length observed for 25 DAC, compared to 40 DAC. Analogously, in other works, it has been shown that the addition of a plasticizer (other than water) leads to less energy absorption by the melt from the screws (*i.e.,* a shear stresses decrease), and preserves fibres from shortening and fibrillation (Peltola, Madsen, Joffe & Nättinen, 2011).

To investigate the effect of injection moulding on fibre shortening, the fibres that were only injection moulded with the highest and lowest moisture contents (injDAC 25 and injDAC 40) were also tested. The fibre length distributions of both these are similar to the unprocessed DAC fibres (Fig. 3b), indicating that the injection moulding process is a milder processing compared to the twin screw extrusion, preserving the fibres from harsh fibre shortening (Table 3).

Overall, after compounding and injection moulding the materials present a lower fibre aspect ratio (Table 3) as a result of both shortening and change in the fibre average width (W_l). The latter can be ascribed to fibre fibrillation and/or agglomeration. Therefore, the higher increase in the average fibre diameter of 25 DAC (from 13 % for 40 DAC and injDAC 25 to 22 % for 25 DAC) is conceivably a result of partial fibrillation due to the relatively higher shear during compounding. Partial fibrillation creates fibres that are more porous and that are extended to higher average widths, but fibres agglomeration could also cause increased diameters. To discern between the two proposed causes of fibre diameter increase, morphological analysis on redispersed fibres after melt processing has been carried out by scanning electron microscopy (SEM).

3.2.4. Microscopy analysis

From the micrographs obtained at lower magnification (250x), the fibres length and the presence of fines can be clearly seen. At higher magnifications (1000x and 2500x) the morphology of the fibres surface and fibrillation can be discerned. The unprocessed material presents long fibres (Fig. 4a) with a low degree of fibrillation (Fig. 4f and k). The fibres redispersed in water from melt compounded materials present shorter fibres and a higher percentage of fines (Fig. 4b for 40 DAC and 4c for 25 DAC).

At higher magnification, the fibres show damaged bundles and increasing fibrillation when the initial moisture content decreases (Fig. 4g-l for 40 DAC and 4h-4 m for 25 DAC), in agreement with the results of the fibre analyser. In the micrographs of fibres redispersed in water from injection moulding, the length seems preserved (Fig. 4d for injDAC 40 and 4e for injDAC 25), and the surface relatively undamaged (Fig. 4i-n for injDAC 40 and Fig. 4j-o for injDAC 25). However, some unfolded bundles can be observed for the injDAC 25, consistently with the larger diameter detected by the fibre analyser. From the microscopy analysis, the decrease in the fibre aspect ratio for compounded materials seem to be more probably related to fibre shortening and fibrillation than agglomeration.

Table 3
Summary of the results obtained by fibre length distribution performed on unprocessed DAC, 40 DAC, 25 DAC, injDAC 40 and injDAC 25: length weighted average length (L_l), percentage of fines ($Fines_l$), length weighted average width (W_l) and aspect ratio.

Material	$Fines_l$ [%]	L_l [mm]	W_l [μm]	Aspect ratio
DAC	12	0.9	23	39
40 DAC	31	0.5	25	22
25 DAC	36	0.4	28	16
injDAC 40	12	0.7	23	28
injDAC 25	11	0.7	25	25

3.2.5. Rheological analyses

Changes in fibre morphology, in particular fibres length and degree of fibrillation, affect the rheological behaviour of fibre dispersions (Schenker, Schoelkopf, Gane & Mangin, 2018, 2019). Therefore, we use rheology to investigate how the fibres and fibre fragments interact with each other in water dispersion, under the rationale that an increase in fibrillation and shortening would result in changes in the water–(nano) fibre interface and (nano)fibre–(nano)fibre supramolecular assembly, *i.e.*, in changes of the dispersions' viscoelastic properties (Fig. 5). The analysis was performed on fibres dispersed in water with a fibre's concentration of 5 wt.%.

Analysis of the variation in storage (G') and loss (G'') moduli as a function of the oscillatory strain provides some conclusions. The linear viscoelastic region (LVR) can be extrapolated; the LVR is represented by the strain domains where the elastic structure of the fibre dispersions remains stable (Nechyporchuk, Belgacem & Pignon, 2016), *i.e.,* the region where the G' and G'' remain strain independent. For all the tested samples, the linearity is maintained up to ~0.3 % shear strain.

Cellulose nanofibres (CNFs) create a gel-like structure in an aqueous medium, due to their assembly in an interconnected network (Nechyporchuk, Belgacem & Pignon, 2016). The gel-like structure is connected to a viscoelastic solid-like behaviour (G' > G'') in the linear viscoelastic region, and to a viscoelastic liquid-like behaviour (G'< G'') beyond a critical shear strain (in this case after 0.3 %), where the fibres network is destroyed (Schenker, Schoelkopf, Gane & Mangin, 2018). Different studies show how more fibrillated fibres create a higher number of mutual interactions between the fibres themselves; those interconnections are related to a higher rigidity of the network (Martoïa et al., 2015). However, network rigidity could also be related to the rigidity of the single network elements (Schenker, Schoelkopf, Gane & Mangin, 2019), *i.e.,* the rigidity of each single fibre. Longer and less fibrillated fibres, like the unprocessed ones, are more rigid, *i.e.* less flexible, than the damaged fibrillated fibres after melt processing. This explains the higher G' values for unprocessed DAC fibres (Fig. 5a). The fibres length, and their integrity, have a greater effect on network elasticity than their fibrillation level, as the values of the G' are reduced progressively with the reduction of the average fibre length (Table 3). Similar conclusions can be drawn considering the dispersions' flow behaviour (Fig. 5b). The fibre length affects the viscosity of the dispersions. A more extensive fibre fibrillation, leading to nanofibril liberation, would create more mutual fibres interaction, *i.e.* higher viscosity (Schenker, Schoelkopf, Gane & Mangin, 2019). Our results suggest partial fibrillation instead. The fibres length and integrity lead to a more rigid network, resulting in higher viscosity up to 5 s^{-1}. All curves show a shear-thinning behaviour; the original fibre network is destroyed, leading the fibres to orient in the flow direction (Yuan, Zeng, Wang, Cheng & Chen, 2021).

Fibres suspended in water tend to flocculate (Beghello, 1998). During the rheological test, while increasing the shear, it has been observed an initial increase, followed by a decrease, in fibre flocs' size (Schenker, Schoelkopf, Gane & Mangin, 2019; Martoïa et al., 2015; Yuan, Zeng, Wang, Cheng, Chen, 2021). This transition can be related to a minimum in the viscosity, at which occur a maximum aggregation, followed by a fibre reorganization (Schenker, Schoelkopf, Gane & Mangin, 2019). In our systems, the local viscosity minima are observed at frequencies higher than 100 s^{-1} and shift to higher shear rates for increased fibre length and decreased degree of fibrillation. Conceivably, long and rigid fibres hinder fibre reorganization.

Overall, the different processing steps lead to fibre dispersions with different rheological behaviour, in agreement with our structural and morphological analysis, being important if considering a possible repulping process.

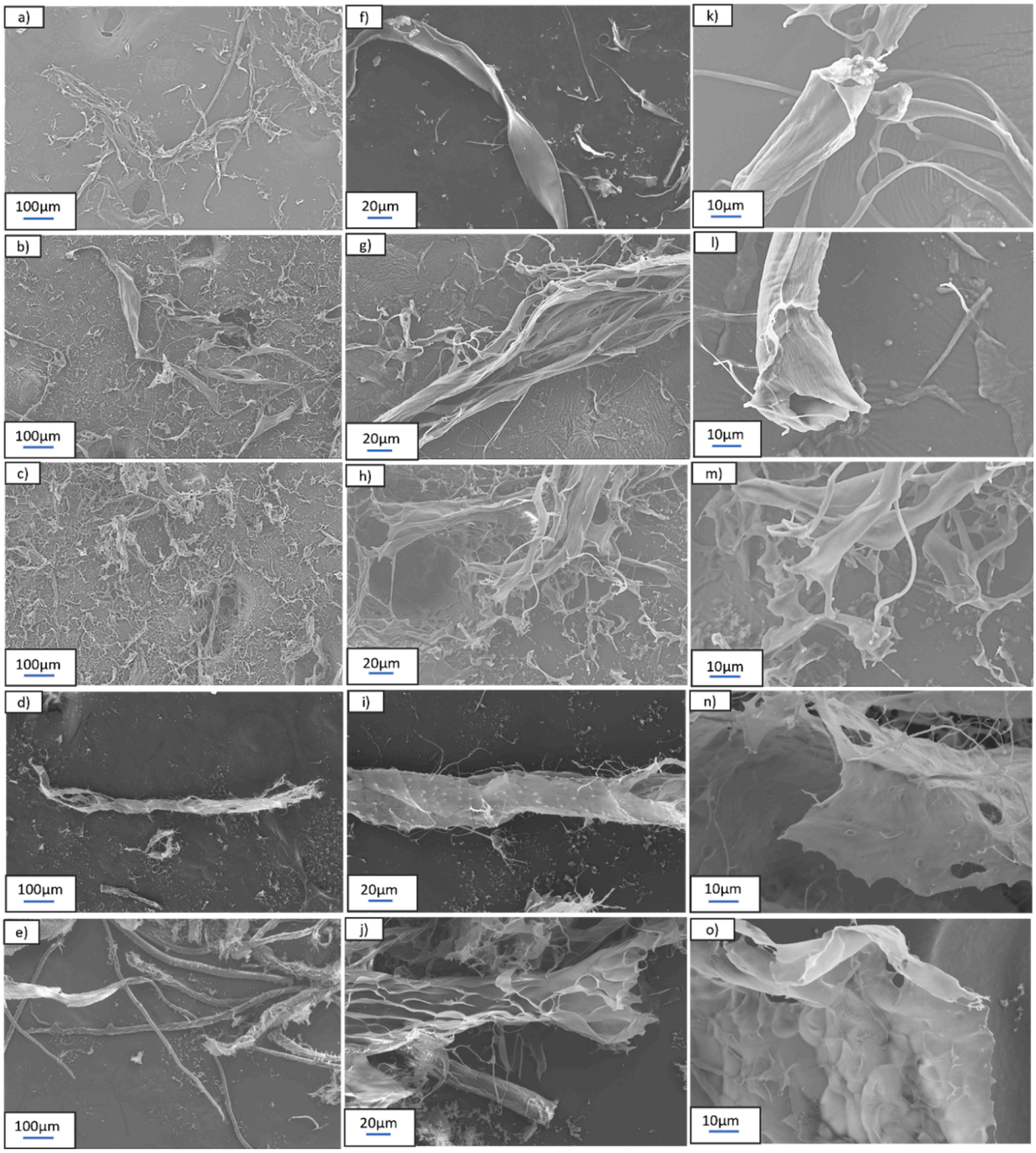

Fig. 4. SEM micrographs of (a, f, k) unprocessed DAC, (b, g, l) 40 DAC, (c, h, m) 25 DAC, (d, i, n) injDAC 40 and (e, j, o) injDAC 25, at different magnification of 250x (left column), 1000x (middle column), 2500x (right column).

3.3. Effect of processing on fibres water drying

Drying measurements were carried out to investigate the effect of the different structures exhibited by the DAC fibres, after different melt processing methods, on the interaction that these materials could have with water. These results can elucidate the different processability of the materials, *i.e.* their injectability, in relation to the structural changes that occurred during the melt processing, due to the role of water as a plasticizer.

Water absorption is an exothermic reaction, *i.e.* wetting Gibbs energy decreases. The decrease in crystallinity leads to a decrease in Gibbs energy upon absorption in nanocellulose (Hollenbeck, Peck & Kildsig, 1978). Water molecules rapidly interact with the cellulose amorphous regions, while crystalline regions remain inaccessible (Froix & Nelson, 1975). Moreover, also morphological changes could affect the surface exposed to water, *i.e.* cellulose-water interactions. (Aulin et.al, 2009). We can speculate that, at the fibre level, a decrease in cellulose crystallinity upon compounding, and the fibrillation of (nano)fibre bundles exposing further amorphous regions, could increase interactions with water molecules.

Processing affects free moisture at the equilibrium (Fig. 6a). It is worth noting that our tests are carried out on samples containing excess water beyond the bounded water. Therefore, we can assume that the free moisture behaviour in time combines an initial linear desorption of excess water (Fig. 6, highlighted by dotted lines) followed by a non-linear desorption of bounded water. The moisture content decreases

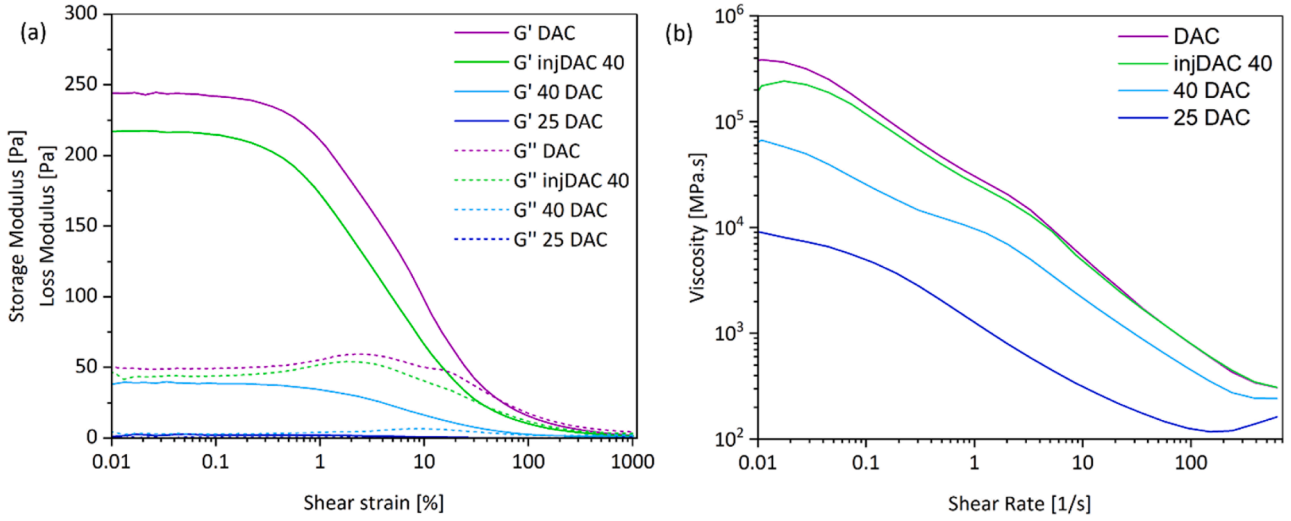

Fig. 5. (a) Storage and Loss modulus as a function of shear strain and (b) viscosity as function of shear rate of 5 wt.% water dispersions of unprocessed DAC and fibres injDAC 40, 40 DAC and 25 DAC.

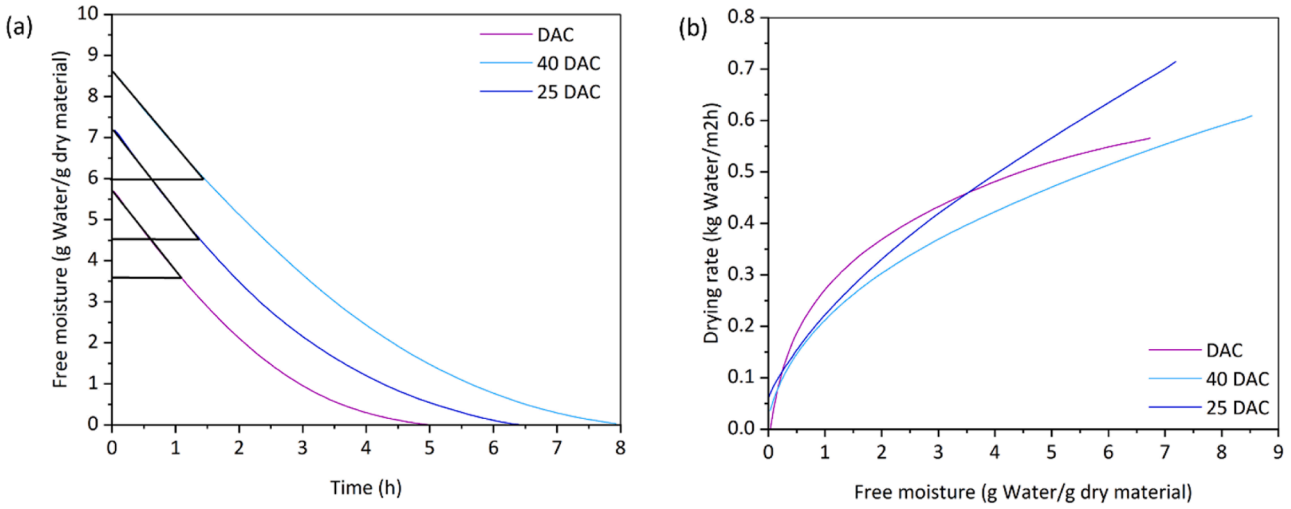

Fig. 6. (a) Moisture content and (b) drying rates of unprocessed DAC fibres, 40 DAC, and 25 DAC. The measurements have been carried out on disks with 26.5 mm diameter and about 300 mg mass.

from 40 DAC to 25 DAC and to DAC. Consistently, the drying rate decreases from DAC to 25 DAC and to 40 DAC. Since fibrillation increases while crystallinity decreases by decreasing the moisture content during compounding, these results suggest an initial increase of fibres surfaces exposed to water in 40 DAC, which leads to larger fibre-water interactions (*i.e.* higher water absorption) and slower water release rate upon drying.

In the case of 25 DAC a higher partial fibrillation could induce higher agglomeration of (nano)fibrils that lowers surface accessibility to the interaction with water (W_l higher for 25 DAC compared to 40 DAC and to DAC, Table 3). The results indicate that moderated changes in crystallinity and fibrillation in 40 DAC open the fibre structure and increase the water interaction, enabling higher water absorption and slower water release. In comparison, a higher decrease in crystallinity and increase in fibrillation observed for 25 DAC, still lead to larger interaction with water compared to unprocessed DAC but reduced compared to the 40 DAC. These results explain why 40 DAC can be injected after compounding, while 25 DAC cannot, despite being both rehydrated with the same moisture content (30 wt.%).

3.4. *Effect of processing on fibres thermomechanical properties*

Assuming negligible the change in density, we studied by dynamic mechanical thermal analysis (DMTA) the influence on the thermomechanical properties in relation to the structural properties changes upon different melt processing steps. The materials melt compounded before injection moulding (40 DAC 30_dir, 40′ DAC 30_ind and 25 DAC 30_ind) exhibit lower storage moduli at any given temperature compared to materials only injected (injDAC 40 and injDAC 25) (Fig. 7a, and Table 3). The lower the fibre aspect ratio after compounding, the lower the mechanical properties of the material. For compounded materials, the method used for injection moulding (direct or indirect) slightly affects the storage moduli. Comparing materials injected without a compounding step, injDAC 25 has lower storage modulus values than injDAC 40 (Table 3). Even for injected DAC, the decrease in the mechanical properties can be attributed to the different fibre length distribution shown by the fibre length analysis (Table 3). The aspect ratio of injDAC 25 is lower compared to injDAC 40, probably due to a higher number of agglomerates preserving fibre length. It is worth noting a slight increase in the storage moduli is observed at higher temperatures (after 160 °C) that can be ascribed to crosslinking

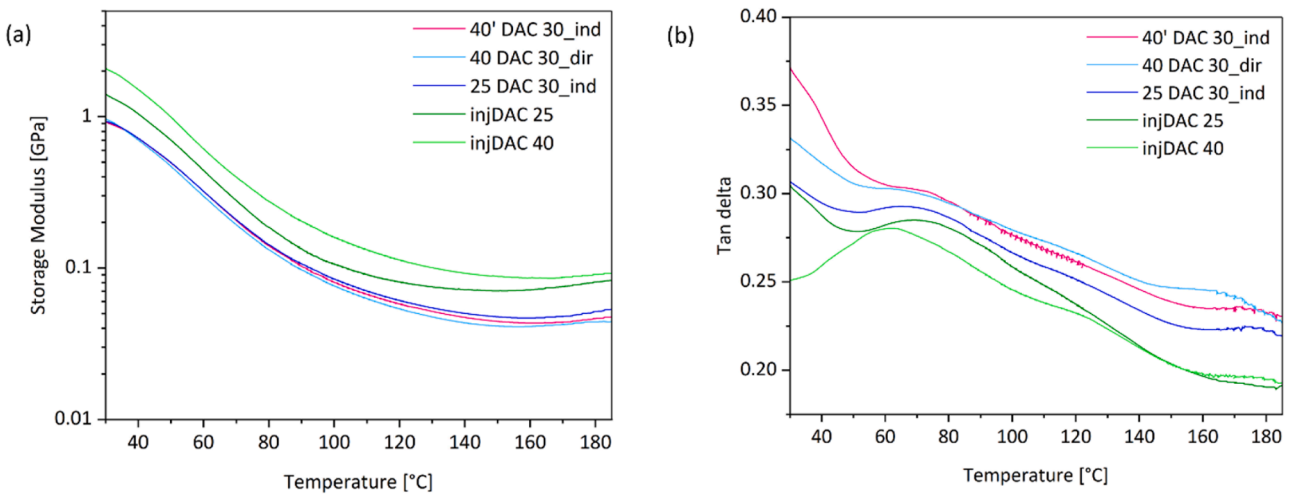

Fig. 7. Variation of Storage Modulus (a) and of the Tan delta with increasing temperature (b) for 40 DAC 30_dir, 40′ DAC 30_ind, 25 DAC 30_ind obtained after melt compounding followed by injection moulding and injDAC 40 and injDAC 25 obtained after the only injection moulding. Note that the initial moisture content of injDAC 40 before the test was 8 %, while was 6 % for the other materials.

reactions induced by extensive water evaporation. During evaporation the water molecules allow for increasing interactions between DAC fibres through hydrogen bonds, creating a multi-hydrogen bonds network. This mechanism could also explain the second transitions visible in the Tan delta at temperatures higher than 160 °C.

The T_g can be estimated from the Tan delta curves (Fig. 7b), indicating the same T_g of 70 °C for all materials except the injDAC 40. This indicates that the different production methods do not affect the relaxation of the amorphous DAC (Table 3) and is consistent with the unchanged molecular weights of the materials after melt processing (Table S2). It is worth noting the only exception: injDAC 40 presents a T_g at a lower temperature, ≈ 63 °C. The materials were conditioned for two days in a chamber at equilibrium conditions (23 °C and 50 % RH) before the test. At these conditions, the moisture content of the materials was evaluated and for all the tested materials it was around 6 % unlike injDAC 40 for which the value is around 8 %. Therefore, the higher amount of water decreases the T_g of injDAC 40 (Salmén & Larsson, 2018).

4. Conclusions

Motivated by the successful use of water as a temporary plasticizer for melt processable dialcohol cellulose (DAC) fibres, this study provides insight into the possibilities and limitations of melt processing techniques relevant to an industrial upscale of 3D-shaped DAC materials as a replacement for fossil-based disposable packaging.

The study evaluates the minimum amount of water required for a stable plasticization of DAC fibres in the two most relevant melt processing processes: extrusion (primary process) and injection moulding (secondary process). All the tested materials were successfully compounded in the extruder, once a minimum initial moisture content needed of 25 wt.% was added. Simulating the production of 3D-shaped materials directly after the pelletization or later in a different industry, we evaluated melt compounding and injection moulding in series (direct) or in separated steps mediated by a rehydration (indirect).

To correlate this experimental evidence of melt processability with structural features of DAC fibres we first assessed no changes in the molecular weight after compounding and injection moulding with different initial moisture contents. Then we evaluated the effect of melt processes on fibres crystallinity and morphology. The initial moisture content (25–40 wt.%) used for the compounding affected the fibres' morphological structure, which determined their ability to be injection moulded. The starting DAC fibres undergoing the primary melt compounding required a minimum moisture content of 40 wt.% to enable their direct and indirect injection moulding.

Melt compounding has shown a destructive effect on fibre crystallinity (evaluated by X-Ray diffraction), fibre shortening and fibrillation (evaluated by fibre length distribution analysis and scanning electron microscopy), having a stronger effect proportional to the decrease in the initial moisture content, *i.e.* under higher viscosities (shear stresses). Compared to extrusion, injection moulding was demonstrated to be a milder melt process for the DAC fibres, preserving more of the initial crystallinity and aspect ratio. Studies of moisture release coupled with thermodynamical considerations enabled to conclude that morphological structural changes during compounding affect the DAC fibres interaction with water. Limited fibrillation and decreased crystallinity in DAC fibres compounded with the higher moisture content (40 wt.%, as shown by 40 DAC) led to higher water absorption and a slower water release. This different interaction with water, due to the milder shear during compounding at higher moisture content, allowed the direct injection of 40 DAC, impossible for lower initial moisture contents.

To close the loop of processes-structure-properties relationships, we correlate changes in the structure caused by the melt processing with the thermo-dynamic mechanical properties of the 3D-injected parts. A reduced DAC fibre aspect ratio lowers the storage moduli in all ranges of temperature investigated, indicating that merely injection moulding (without any prior compounding) is the most suitable melt process to obtain materials with higher mechanical properties. The material only injected with the highest water content (40 wt.%, as for injDAC40) demonstrated a storage modulus larger than 2 GPa at 30 °C, superior to most of the fossil-based low- or high-density polyethylene, ranging from 0.6 to 1.5 GPa, respectively.

Furthermore, as a recycling path at the end-of-life of 3D-parts, DAC fibres were successfully resuspended in water, and the rheological behaviour of the suspensions indicated their potential for repulping process, further contributing to DAC fibres-based materials' sustainability.

CRediT authorship contribution statement

Enrica Pellegrino: Writing – original draft, Visualization, Investigation, Formal analysis, Data curation. **Basel Al-Rudainy:** Investigation, Formal analysis, Data curation. **Per A. Larsson:** Writing – review & editing, Validation, Supervision. **Alberto Fina:** Writing – review & editing, Validation, Supervision. **Giada Lo Re:** Writing – review & editing, Validation, Supervision, Software, Resources, Project

administration, Methodology, Funding acquisition, Formal analysis, Conceptualization.

Declaration of competing interest

The authors declare that they have no known competing financial interests or personal relationships that could have appeared to influence the work reported in this paper titled "Impact of water plasticization on dialcohol cellulose fibres melt processing-structure-properties in 3D-shaped materials".

Acknowledgements

The authors acknowledge Tetra Pak and Treesearch for funding and in-kind support, as well as BillerudKorsnäs for in-kind support. The authors acknowledge VINNOVA through the project BioInnovation ProDAC (grant number 2021-02094) for financial support, and FibRe (grant number 2019-00047).

Supplementary materials

Supplementary material associated with this article can be found, in the online version, at doi:10.1016/j.carpta.2024.100642.

Data availability

Data will be made available on request.

References

Aulin, C., Ahola, S., Josefsson, P., Nishino, T., Hirose, Y., Osterberg, M., & Wagberg, L. (2009). Nanoscale cellulose films with different crystallinities and mesostructures-their surface properties and interaction with water. *Langmuir : The ACS Journal of Surfaces and Colloids, 25*(13), 7675–7685.

Beghello, L. (1998). Some factors that influence fiber flocculation. *Nordic Pulp & Paper Research Journal, 13*(4), 274–279.

Carvalho, M. G., Ferreira, P. J., Martins, A. A., & Figueiredo, M. M. (1997). A comparative study of two automated techniques for measuring fiber length. *Tappi Journal*, (2), 137–142.

Emsley, A. M., Ali, M., & Heywood, R. J. (2000). A size exclusion chromatography study of cellulose degradation. *Polymer, 41*(24), 8513–8521.

Engel, E. R., Lo Re, G., & Larsson, P. A. (2024). Melt processing of chemically modified cellulosic fibres with only water as plasticiser: Effects of moisture content and processing temperature. *Carbohydrate Polymers*, Article 122891.

European Bioplastics 2021, Available, www.european-bioplastics.org.

French, A. D. (2014). Idealized powder diffraction patterns for cellulose polymorphs. *Cellulose (London, England), 21*(2), 885–896.

Froix, M. F., & Nelson, R. (1975). The interaction of water with cellulose from nuclear magnetic resonance relaxation times. *Macromolecules, 8*(6), 726–730.

Guigo, N., Mazeau, K., Putaux, J. L., & Heux, L. (2014). Surface modification of cellulose microfibrils by periodate oxidation and subsequent reductive amination with benzylamine: A topochemical study. *Cellulose (London, England), 21*, 4119–4133.

Hollenbeck, R. G., Peck, G. E., & Kildsig, D. O. (1978). Application of immersional calorimetry to investigation of solid–liquid interactions: Microcrystalline cellulose–water system. *Journal of Pharmaceutical Sciences, 67*(11), 1599–1606.

Kasai, W., Morooka, T., & Ek, M. (2014). Mechanical properties of films made from dialcohol cellulose prepared by homogeneous periodate oxidation. *Cellulose (London, England), 21*(1), 769–776.

Larsson, P. A., Berglund, L. A., & Wågberg, L. (2014). Highly ductile fibres and sheets by core-shell structuring of the cellulose nanofibrils. *Cellulose (London, England), 21*(1), 323–333.

Larsson, P. A., Gimåker, M., & Wågberg, L. (2008). The influence of periodate oxidation on the moisture sorptivity and dimensional stability of paper. *Cellulose (London, England), 15*(6), 837–847.

Larsson, P. A., & Wågberg, L. (2016). Towards natural-fibre-based thermoplastic films produced by conventional papermaking. *Green Chemistry, 18*(11), 3324–3333.

Li, C., Wu, J., Shi, H., Xia, Z., Sahoo, J. K., Yeo, J., & Kaplan, D. L. (2022). Fiber-based biopolymer processing as a route toward sustainability. *Advanced Materials, 34*(1), Article 2105196.

Liu, Y., Ahmed, S., Sameen, D. E., Wang, Y., Lu, R., Dai, J., & Qin, W. (2021). A review of cellulose and its derivatives in biopolymer-based for food packaging application. *Trends in Food Science & Technology, 112*, 532–546.

Li, Y., Yan, C., Chen, Y., Han, X., Shao, Z., Qi, H., Li, X., Nishiyama, Y., Hu, T., & Chen, P. (2023). The major role of London dispersion interaction in the assembly of cellulose, chitin, and chitosan. *Cellulose (London, England), 30*(13), 8127–8138.

Lo Re, G., Engel, E. R., Björn, L., Sicairos, M. G., Liebi, M., Wahlberg, J., Jonasson, K., & Larsson, P. A. (2023). Melt processable cellulose fibres engineered for replacing oil-based thermoplastics. *Chemical Engineering Journal*, Article 141372.

Martínez-Sanz, M., Pettolino, F., Flanagan, B., Gidley, M. J., & Gilbert, E. P. (2017). Structure of cellulose microfibrils in mature cotton fibres. *Carbohydrate Polymers, 175*, 450–463.

Martoïa, F., Perge, C., Dumont, P. J. J., Orgéas, L., Fardin, M. A., Manneville, S., & Belgacem, M. N. (2015). Heterogeneous flow kinematics of cellulose nanofibril dispersions under shear. *Soft Matter, 11*(24), 4742–4755.

Mehandzhiyski, A. Y., Engel, E., Larsson, P. A., Lo Re, G., & Zozoulenko, I. V. (2022). Microscopic Insight into the Structure–Processing–Property Relationships of Core–Shell Structured Dialcohol Cellulose Nanoparticles. *ACS Applied Bio Materials, 5*(10), 4793–4802.

Mystek, K., Li, H., Pettersson, T., Françon, H., Svagan, A. J., Larsson, P. A., & Wågberg, L. (2020). Wet-expandable capsules made from partially modified cellulose. *Green Chemistry, 22*(14), 4581–4592.

Mohtaschemi, M., Sorvari, A., Puisto, A., Nuopponen, M., Seppälä, J., & Alava, M. J. (2014). The vane method and kinetic modeling: Shear rheology of nanofibrillated cellulose dispersions. *Cellulose (London, England), 21*, 3913–3925.

Mörseburg, K., Hultholm, T., Lundin, T., & Lönnberg, B. (1999). Experiences with the Kajaani FiberLab Analyzer in determining morphological characteristics of mechanical and chemical pulps. In *In 5th PTS-Symp* (p. 13). -1.

Münster, L., Vícha, J., Klofáč, J., Masař, M., Kucharczyk, P., & Kuřitka, I. (2017). Stability and aging of solubilized dialdehyde cellulose. *Cellulose (London, England), 24*, 2753–2766.

Nechyporchuk, O., Belgacem, M. N., & Pignon, F. (2016). Current progress in rheology of cellulose nanofibril dispersions. *Biomacromolecules, 17*(7), 2311–2320.

Park, S., Baker, J. O., Himmel, M. E., Parilla, P. A., & Johnson, D. K. (2010). Cellulose crystallinity index: Measurement techniques and their impact on interpreting cellulase performance. *Biotechnology for Biofuels, 3*, 1–10.

Peltola, H., Madsen, B., Joffe, R., & Nättinen, K. (2011). Experimental study of fiber length and orientation in injection molded natural fiber/starch acetate composites. *Advances in Materials Science and Engineering*.

Salmén, L., & Larsson, P. A. (2018). On the origin of sorption hysteresis in cellulosic materials. *Carbohydrate Polymers, 182*, 15–20.

Schenker, M., Schoelkopf, J., Gane, P., & Mangin, P. (2018). Influence of shear rheometer measurement systems on the rheological properties of microfibrillated cellulose (MFC) dispersions. *Cellulose (London, England), 25*, 961–976.

Schenker, M., Schoelkopf, J., Gane, P., & Mangin, P. (2019). Rheology of microfibrillated cellulose (MFC) dispersions: Influence of the degree of fibrillation and residual fibre content on flow and viscoelastic properties. *Cellulose (London, England), 26*, 845–860.

Schroeter, J., & Felix, F. (2005). Melting cellulose. *Cellulose (London, England), 12*, 159–165.

Segal, L. G. J. M. A., Creely, J. J., Martin, A. E., Jr, & Conrad, C. M (1959). An empirical method for estimating the degree of crystallinity of native cellulose using the X-ray diffractometer. *Textile Research Journal, 29*(10), 786–794.

Simon, J., Fliri, L., Fröhlich, F., Sapkota, J., Ristolainen, M., Hummel, M., … Potthast, A. (2023). Insights into the borohydride reduction of dialdehyde cellulose: The dilemma of competing reduction and β-elimination reactions. *Cellulose (London, England), 30*(13), 8205–8220.

Statista 2021 https://www.statista.com/statistics/282732/global-production-of-plastics-since-1950/.

Westermark, U., & Gustafsson, K. (1994). Molecular size distribution of wood polymers in birch kraft pulps.

Wohlert, J., Chen, P., Berglund, L. A., & Lo Re, G. (2023). Acetylation of nanocellulose: Miscibility and reinforcement mechanisms in polymer nanocomposites. *ACS Nano*.

Wu, J., Bai, J., Xue, Z., Liao, Y., Zhou, X., & Xie, X. (2015). Insight into glass transition of cellulose based on direct thermal processing after plasticization by ionic liquid. *Cellulose (London, England), 22*, 89–99.

Yuan, T., Zeng, J., Wang, B., Cheng, Z., & Chen, K. (2021). Cellulosic fiber: Mechanical fibrillation-morphology-rheology relationships. *Cellulose (London, England), 28*, 7651–7662.

Zeronian, S. H., Hudson, F. L., & Peters, R. H. (1964). The mechanical properties of paper made from periodate oxycellulose pulp and from the same pulp after reduction with borohydride. *Tappi, 47*, 557–564.

Zhang, X., Wu, X., Gao, D., & Xia, K. (2012). Bulk cellulose plastic materials from processing cellulose powder using back pressure-equal channel angular pressing. *Carbohydrate Polymers, 87*(4), 2470–2476.

Zhao, H., & Heindel, N. D. (1991). Determination of degree of substitution of formyl groups in polyaldehyde dextran by the hydroxylamine hydrochloride method. *Pharmaceutical research, 8*, 400–402.